O VII TRIPLET IN SEYFERT GALAXIES: THE *Chandra* GRATINGS VIEW

R. Morales[a], M. Elvis[a], F. Nicastro[a], A. Fruscione[a] and E. Galle [a]

[a]Harvard-Smithsonian Center for Astrophysics, 60 Garden Street, Cambridge, MA 02138 USA

The O VII triplet plasma diagnostic is applied to *Chandra* observations of all Seyfert galaxies publicly available by Nov. 15th 2002. The results for the electron density, n_e, upper limit for four Type 1 Seyfert galaxies ranges from 4×10^9 to 4×10^{10} cm^{-3}; for the NGC1068 Type 2 Seyfert galaxies, $n_e < 5 \times 10^{10}$ cm^{-3}.

1. Introduction

With the advent of a new generation of X-ray satellites (*Chandra* and *XMM-Newton*), X-ray spectroscopy for extra-solar objects with unprecedent spectral resolution is now possible for the first time. Various plasma diagnostics are accessible such as those based on the line ratios of He-like triplets. The He-like triplet ratios diagnostics are a powerful tool in the analysis of high-resolution spectra of a variety of plasmas, such as collisional, photoionized, hybrid and out of equilibrium (e.g. see contributions by Manuel Güdel and Jurgen Schmitt in this volume). In particular, diagnostics based on line ratios of He-like ions have been first applied to Seyfert galaxies (e.g. [1]).

In this contribution we apply the O VII triplet plasma diagnostics to *Chandra* observations of all Seyfert galaxies publicly available by Nov. 15th 2002. Section 2 describes the technique of He–like triplet plasma diagnostics and explains the choice of the O VII triplet for our study. The data sample, spectral analysis and results are presented in Section 3. Finally a discussion of our results and their consequences are summarized in Section 4.

2. He–like triplet plasma diagnostics

Fig. 1 presents a Grotrian diagram showing all transitions within the O VII triplet. The excited states ($1s2l$) split up into several terms, out of which the levels with $J \neq 0$ decay to the ground state through the resonance, intercombination and forbidden lines. The intercombination and forbidden lines involve spin changes, and therefore violate the selection rules for electric dipole radiation. Although the radiative transition rate for the forbidden line is quite small, in a low density plasma (e.g. $n_e \leq 10^9$ cm^{-3} for the O VII triplet) collisional de-population processes are so rare that the excited state does radiatively decay. In a high density plasma (e.g. $n_e \geq 10^{12}$ cm^{-3} for the O VII triplet), collisional de-excitations dominate and hence the forbidden line disappears.

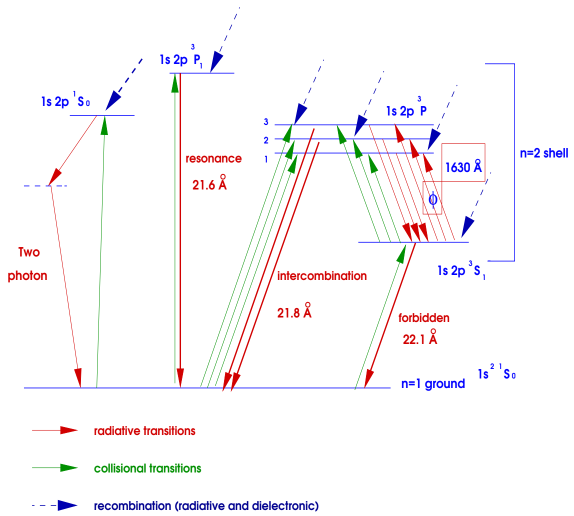

Figure 1. The He–like transitions, showing those terms and processes involved in the He–like triplet plasma diagnostics. The wavelengths indicated apply to the case of O VII. Adapted from [2].

The techniques to determine the electron density, n_e, and the electron temperature, T_e, use the ratios:

$$R(n_e) = \frac{f}{i} \quad (1)$$

$$G(T_e) = \frac{f+i}{r} \quad (2)$$

where f, i and r stand for the intensities of the

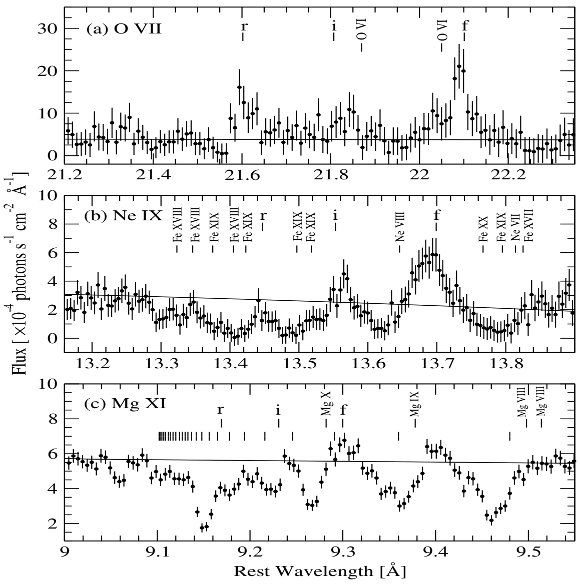

Figure 2. Emission lines from He-like ion triplets in the 900 ksec *Chandra* HETG observation of NGC 3783 from [3]. Panel (a): OVII from the MEG binned to 0.01 Å. Panel (b): NeIX from the MEG binned to 0.005 Å. Panel (c): MgXI from the MEG+HEG binned to 0.005 Å. The fitted local continuum is plotted as a solid line in each panel. In (b) and (c) the lines blended with the triplets are marked. The un-labeled vertical marks in (c) denote the NeX lines which are blended with the MgXI triplet. All lines are marked at their rest wavelengths.

forbidden, intercombination and resonance lines. These ratios were first introduced in the analysis of the solar coronae [2]. For low density plasmas, the relative intensities of the three lines are independent of density and R is approximately constant. As n_e increases, f decreases while i increases. Therefore, R decreases over 2 or 3 decades of n_e. For much higher densities the resonance line becomes sensitive to density.

These diagnostics of He–like triplets have strong advantages. The lines are emitted by the same ionization stage of one element, thus eliminating any uncertainties due to elemental abundances. In addition, since the line energies are relatively close together, wavelength dependent instrumental calibration uncertainties are minimal.

2.1. Choice of the OVII triplet

The aim for this study is to apply the He–like triplet plasma diagnostics on as many objects as available in the *Chandra* archival. In the *Chandra* spectrum there are several He–like triplets we could have used, but as seen in Fig.2, the OVII triplet is the only one which is almost free from blends by nearby lines.

3. OVII triplet in Seyfert galaxies

3.1. Data sample and data reduction

Our sample consists of all observations of Type 1 and 2 Seyfert galaxies publicly available in the *Chandra* archive[1] by November 15$^{\text{th}}$ 2002. This makes up a total of 33 observations of 22 different objects. The observations are listed in Table 1.

In order to reduce all these observations, we have built two scripts to produce fluxed grating spectra. Both scripts work for all instrument/grating combinations. The output files are all in FITS.

The first script combines existing CIAO *threads*[2] (each of which uses several CIAO tools) to extract grating spectra from event files using the latest calibrations[3], rather than those in the archive products which use less reliable calibrations from the epoch of processing. For these faint sources the plus and minus first orders are co-added, and an average ARF is produced.

The second script divides the extracted spectrum by the corresponding ARF and groups MEG spectra by a factor of 5 (LETG spectra are unbinned). Finally, the data is de-redshifts to make a final fluxed, rest-frame, spectrum.

3.2. Isolating the triplet: spectral analysis

To measure lines fluxes, one first needs to define the continuum shape and level. The method we have chosen to apply has been to fit the local continuum to a 4th degree polynomial and the r, i and f lines with three Gaussians. The fitting package used has been Sherpa Version: 2.3[4].

The local continuum is defined to be between 20 and 24 Å. Given that the strongest line in all the spectra is the f line, we have fixed the redshift, and the FWHM of the i and r lines to those values observed for f (i.e. we made the assumption that the three lines are produced by the same

[1] http://cxc.harvard.edu/cda/
[2] http://cxc.harvard.edu/ciao/threads/index.html
[3] http://cxc.harvard.edu/caldb/
[4] http://cxc.harvard.edu/ciao/threads/sherpa.html

Table 1: OBSERVATIONS DESCRIPTION

obsid	Source	exposure (ksec)	instrument	Optical z ($\mathrm{km\,s^{-1}}$)	Optical z Reference
1594	1ES1927+654	60	HRC-S LETG	5096	[4]
1600	CENTAURUS A	50	ACIS-S HETG	547	[5]
1601		50	ACIS-S HETG		
374	CIRC GAL	8	ACIS-S HETG	449	[6]
62877		67	ACIS-S HETG		
2088	FAIRALL 9	80	ACIS-S HETG	14095	[7]
2177	IC 4329A	60	ACIS-S HETG	4813	[8]
433	MCG–6-30-15	125	ACIS-S HETG	2323	[9]
873	MKN 3	100	ACIS-S HETG	4050	[10]
2087	MKN 509	60	ACIS-S HETG	10312	[9]
1597	MKN 766	90	ACIS-S HETG	3876	[11]
329	NGC1068	80	ACIS-S LETG	1137	[12]
332		50	ACIS-S HETG		
333	NGC1275	50	ACIS-S HETG	5264	[13]
428		25	ACIS-S HETG		
860	NGC3227	50	ACIS-S HETG	1157	[14]
1591		100	HRC-S LETG		
831	NGC3516	50	ACIS-S LETG	2649	[15]
373	NGC3783	55	ACIS-S HETG	2917	[16]
2090		170	ACIS-S HETG		
2091		170	ACIS-S HETG		
2092		170	ACIS-S HETG		
2093		170	ACIS-S HETG		
2094		170	ACIS-S HETG		
859	NGC4051	80	ACIS-S HETG	725	[17]
335	NGC4151	50	ACIS-S HETG	995	[14]
810	NGC4258	150	HRC-S LETG	448	[14]
2150	NGC4507	140	ACIS-S HETG	3538	[18]
1589	NGC4593	120	HRC-S LETG	2698	[13]
2089		80	ACIS-S HETG		
1598	NGC5506	90	ACIS-S HETG	1853	[15]
330	NGC5548	80	HRC-S LETG	5149	[14]
837		80	ACIS-S HETG		

gas). This procedure ensures that we do not underestimate the width of the i and r lines, and also that we do not misidentify any of the triplet lines. No other absorption or emission lines have been considered at this stage of our analysis.

3.3. Placement of the continuum

A big concern in our work is the correct assessment for the placement of the continuum. Small variations lead to changes on R, and therefore, might alter the evaluation of n_e[19]. We have used the 900ksec observation of NGC 3783[5] to study the impact of various continuum levels on the values of R and n_e [20]. Our results are given in Table 2, which also reports the values obtained when the local continuum is determined using the line free zones (LFZ). The LFZ have been chosen by eliminating the triplet lines and the resonance absorption lines [21]. For that, each line has been allowed to have a velocity dispersion of 600 km s^{-1}. The last entry on Table 2 corresponds to considering [22] continuum. Fig. 3 illustrates a comparison of the R and n_e values obtained. Note that within the error bars, the results are consistent with each other.

3.4. Results

Only those observations with high enough S/N can be used to determine the FWHM, the redshift of the lines with respect to optical lines and the flux in the lines. For a total of 9 objects, we have found f to be detected at a 3σ level or higher. All the observations of these objects have been considered in our analysis: a total of 18 observations. Table 3 gives the values of the FWHM and the redshift for the forbidden line. Table 4 presents the flux in the triplet lines, the R value and the upper limit for the electron density, n_e, as deduced from comparison with [19].

4. Discussion

The most striking result of our study, illustrated in Fig. 4, is that the FWHM and the flux of the lines seem to be different for Type 1 and Type 2 Seyfert galaxies. The mean FWHM for Seyfert 1 galaxies is $\sim 600 \pm 300$ km s^{-1}, while for Seyfert 2 galaxies the mean FWHM is $\sim 1230 \pm 200$ km s^{-1}. The n_e upper limit for Type 1 Seyfert galaxies, given from the R ratio, is constrained for 4 objects. It ranges from 4×10^9 to 4×10^{10} cm^{-3}. For the three Type 2 Seyfert galaxies, only the NGC1068 R value is constrained and gives $n_e < 5 \times 10^{10}$ cm^{-3}.

[5]The 900ksec observation has been obtained by co-adding five NGC3783 observations, which obsids are 2090, 2091, 2092, 2093, and 2094.

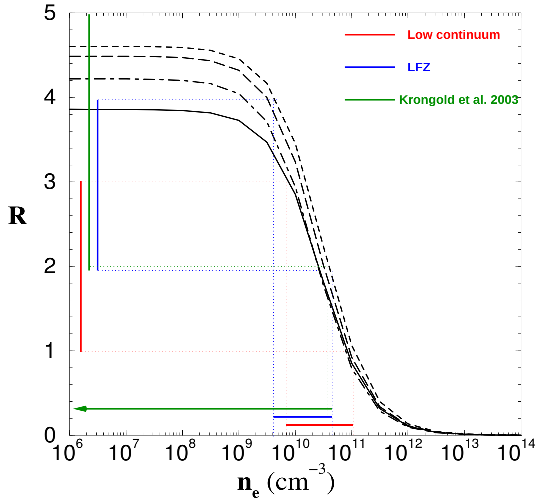

Figure 3. R versus n_e for a pure photoionized plasma from [19]. The black solid line corresponds to $T_e = 10^5$K, the black dash-dot line to $T_e = 5 \times 10^5$K, the black dashed line to $T_e = 10^6$K, and the small dashed line to $T_e = 1.8 \times 10^6$K. In red, blue and green are indicated the NGC3783 900 ksec observation R values obtained for the low continuum, LFZ and [22] continuum, respectively – see main text and Table 2 for explanation. Also, the corresponding n_e values are marked in the same color code.

REFERENCES

1. Kaastra, J. S., Mewe, R., Liedahl, D. A., Komossa, S., & Brinkman, A. C. 2000, A&A, 354, L83
2. Gabriel, A. H. & Jordan, C. 1969, MNRAS, 145, 241
3. Kaspi, S., Brandt, W. N., George, I. M., Netzer, H., Crenshaw, D. M., Gabel, J. R., Hamann, F. W., Kaiser, M. E., Koratkar, A., Kraemer, S. B., Kriss, G. A., Mathur, S., Mushotzky, R. F., Nandra, K., Peterson, B. M., Shields, J. C., Turner, T. J., & Zheng, W. 2002, ApJ, 574, 643
4. Veron-Cetty, M. . & Veron, P. 1989, "A Catalogue of quasars and active nuclei" (ESO Scientific Report, Garching: European Southern Observatory (ESO), 1989, 4th ed.)
5. Graham, J. A. 1978, PASP, 90, 237

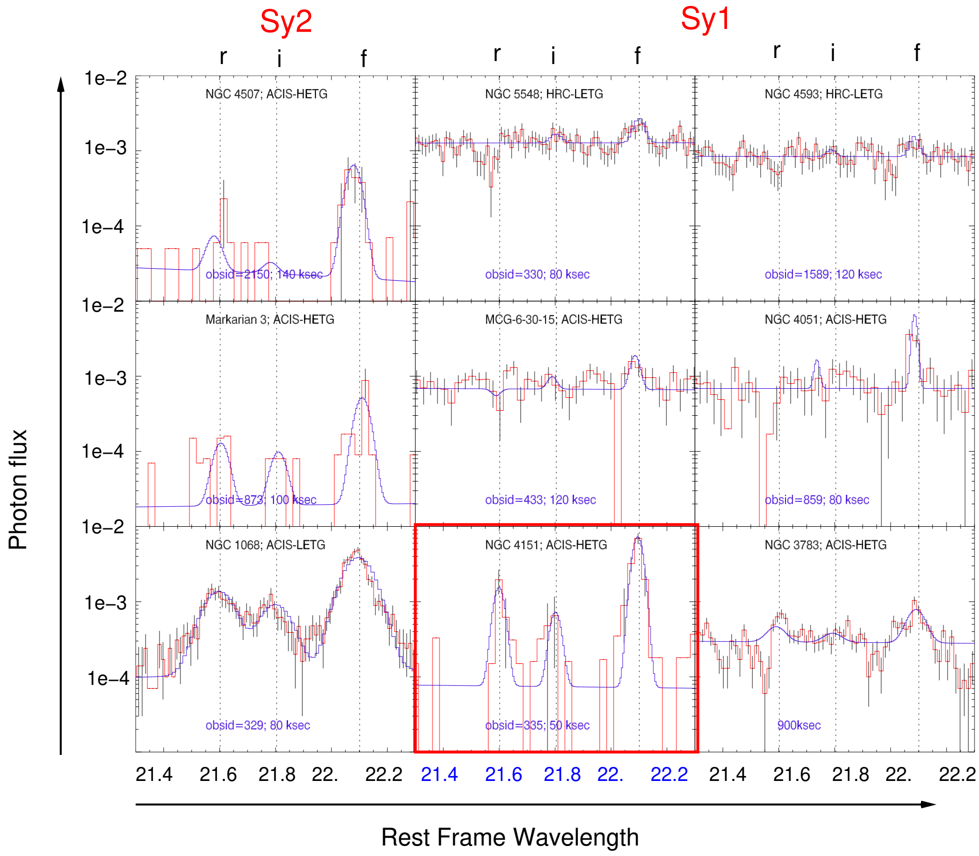

Figure 4. Comparison of 9 observations of the 9 objects with higher S/N detection for the forbidden line. The photon flux is in ph cm $^{-2}$s $^{-1}$Å^{-1} and the rest wavelength in Å. The observation description appears at the top and bottom of each panel. The positions of the resonance, intercombination and forbidden lines are marked with black dotted lines and labeled r, i and f respectively. The first column shows three Seyfert 2 galaxies and the other two columns show Seyfert 1 galaxies. NGC 4151 in the last row, appears in a red square, since it is a Type 1.5 Seyfert.

6. Juraszek, S. J., Staveley-Smith, L., Kraan-Korteweg, R. C., Green, A. J., Ekers, R. D., Haynes, R. F., Henning, P. A., Kesteven, M. J., Koribalski, B., Price, R. M., Sadler, E. M., & Schröder, A. 2000, AJ, 119, 1627
7. Lauberts, A. & Valentijn, E. A. 1989, The surface photometry catalogue of the ESO-Uppsala galaxies (Garching: European Southern Observatory, —c1989)
8. Willmer, C. N. A., Focardi, P., Chan, R., Pellegrini, P. S., & da Costa, N. L. 1991, AJ, 101, 57
9. Fisher, K. B., Huchra, J. P., Strauss, M. A., Davis, M., Yahil, A., & Schlegel, D. 1995, ApJS, 100, 69+
10. Tift, W. G. & Cocke, W. J. 1988, ApJS, 67, 1
11. Smith, B. J., Kleinmann, S. G., Huchra, J. P., & Low, F. J. 1987, ApJ, 318, 161
12. Huchra, J. P., Vogeley, M. S., & Geller, M. J. 1999, ApJS, 121, 287
13. Strauss, M. A., Huchra, J. P., Davis, M., Yahil, A., Fisher, K. B., & Tonry, J. 1992, ApJS, 83, 29
14. de Vaucouleurs, G., de Vaucouleurs, A., Corwin, H. G., Buta, R. J., Paturel, G., & Fouque, P. 1991, S&T, 82, 621
15. Keel, W. C. 1996, ApJS, 106, 27
16. Theureau, G., Bottinelli, L., Coudreau-Durand, N., Gouguenheim, L., Hallet, N., Loulergue, M., Paturel, G., & Teerikorpi, P. 1998, A&AS, 130, 333

TABLE 4. OVII TRIPLET LINES FLUXES, R AND n_e VALUES

Source	obsid	Type	r$^{(1)}$	i$^{(1)}$	f$^{(1)}$	R	n_e cm^{-3}
MCG–6-30-15	433	1	-0.5 ± 0.8	1.3 ± 1.0	5.0 ± 1.4	4 ± 4	unconstrained
MKN 3	873	2	0.7 ± 0.4	0.5 ± 0.4	3.2 ± 0.9	6 ± 7	unconstrained
NGC3783	900ksec	1	1.4 ± 0.3	0.7 ± 0.3	4.0 ± 0.5	5 ± 3	$< 4 \times 10^{10}$
	373		2.4 ± 1.3	1.5 ± 1.2	5.8 ± 2.0	4 ± 5	unconstrained
	2090		3.5 ± 0.8	1.6 ± 0.7	4.4 ± 0.9	3 ± 2	$< 1 \times 10^{11}$
	2091		2.0 ± 0.7	1.0 ± 0.7	4.7 ± 1.0	5 ± 4	$< 1 \times 10^{11}$
	2092		0.5 ± 0.5	0.0 ± 0.4	2.7 ± 0.8	< 6.7	unconstrained
	2093		0.0 ± 3.8	1.4 ± 2.1	3.7 ± 1.5	3 ± 5	unconstrained
	2094		8.4 ± 3.7	0.0 ± 4.0	10.2 ± 9.0	< 2.5	$> 4 \times 10^{9}$
NGC4051	859	1	0 ± 1	2.3 ± 1.0	13 ± 2	5.6 ± 3.3	$< 4 \times 10^{9}$
NGC4151	335	1.5	6.7 ± 1.7	3.0 ± 1.3	32.9 ± 3.9	11 ± 6	unconstrained
NGC1068	329	2	16.9 ± 1.0	10.8 ± 0.8	50.2 ± 1.7	5 ± 1	$< 5 \times 10^{10}$
	332		22.2 ± 3.2	7.4 ± 2.1	54.7 ± 5.2	7 ± 3	$< 5 \times 10^{10}$
NGC4507	2150	2	0.3 ± 0.4	0.1 ± 0.2	4.0 ± 0.8	< 20	unconstrained
NGC4593	1589	1	0.0 ± 0.8	0.8 ± 0.7	2.8 ± 0.8	4 ± 4	unconstrained
	2089		0.1 ± 1.1	0.0 ± 1.1	4.5 ± 1.5	< 4	$> 5 \times 10^{9}$
NGC5548	330	1	0.0 ± 1.0	1.9 ± 1.0	6.8 ± 1.3	4 ± 3	$< 1 \times 10^{11}$
	837		0.0 ± 1.0	2.8 ± 1.3	9.9 ± 2.2	4 ± 2	$< 4 \times 10^{10}$

(1) $\times 10^{-5}$ (ph cm^{-2}s^{-1})

TABLE 3. OVII FORBIDDEN LINE FWHM AND $\Delta\lambda$

Source	obsid	FWHM (km s^{-1})	$\Delta\lambda$ (km s^{-1})
MCG–6-30-15	433	520 ± 211	238 ± 93
MKN 3	873	823 ± 225	-91 ± 116
NGC3783	900ksec	1000 ± 174	175 ± 77
	373	335 ± 161	-11 ± 80
	2090	793 ± 134	64 ± 93
	2091	980 ± 265	190 ± 103
	2092	310 ± 178	170 ± 67
	2093	1316 ± 1331	549 ± 392
	2094	360 ± 843	-208 ± 389
NGC4051	859	285 ± 69	239 ± 27
NGC4151	335	580 ± 65	109 ± 35
NGC1068	329	1700 ± 49	152 ± 27
	332	1584 ± 121	544 ± 70
NGC4507	2150	809 ± 150	329 ± 80
NGC4593	1589	505 ± 299	315 ± 130
	2089	227 ± 176	87 ± 60
NGC5548	330	608 ± 216	100 ± 89
	837	608 ± 201	320 ± 79

TABLE 2. NGC3783 900KSEC OVII TRIPLET FLUXES FOR ALTERNATIVE CONTINUUM CHOICES

(1)	r$^{(2)}$	i$^{(2)}$	f$^{(2)}$	R	$n_e \times 10^{10}$ cm^{-3}
high$^{(3)}$	0.9 ± 0.2	0.2 ± 0.3	2.8 ± 0.5	14 ± 23	$^{(4)}$
medium$^{(5)}$	1.4 ± 0.3	0.7 ± 0.3	4.0 ± 0.5	6 ± 3	< 0.8
low$^{(6)}$	2.5 ± 0.4	2.3 ± 0.4	5.7 ± 0.5	2 ± 1	4 ± 6
LFZ$^{(7)}$	1.9 ± 0.4	1.6 ± 0.4	5.0 ± 0.5	3 ± 1	$0.8^{+0.6}_{-0.3}$
Krongold$^{(8)}$	4.5 ± 0.4	1.3 ± 0.4	4.8 ± 0.5	4 ± 2	< 5

(1) Continuum level
(2) $\times 10^{-5}$ (ph cm^{-2}s^{-1})
(3) Continuum level 5% higher than that given by the Sherpa fit.
(4) R is not constrained.
(5) Continuum level given by the Sherpa fit.
(6) Continuum level 8% lowerer than that given by the Sherpa fit.
(7) Line Free Zone continuum level.
(8) [22] continuum.

17. Verheijen, M. A. W. & Sancisi, R. 2001, A&A, 370, 765
18. Aguero, E. L., Suarez, F., & Paolantonio, S. 1995, PASP, 107, 959
19. Porquet, D. & Dubau, J. 2000, A&AS, 143, 495
20. Morales, R., Nicastro, F. & Elvis, M. 2003, ApJ, in preparation.
21. Verner, D. A., Verner, E. M., & Ferland, G. J. 1996, in American Astronomical Society Meeting, Vol. 188, 5418+
22. Krongold, Y., Brickhouse, N. S., Nicastro, F. & Elvis, M. 2003, ApJ, in preparation.

ACKNOWLEDGMENTS

The authors want to thank Yair Krongold for providing his NGC 3783 modeling and Norbert S. Schulz for a careful reading of the manuscript and useful comments.